

# MICU1 Motifs Define Mitochondrial Calcium Uniporter Binding and Activity

Nicholas E. Hoffman,<sup>1,2,7</sup> Harish C. Chandramoorthy,<sup>1,2,6,7</sup> Santhanam Shamugapriya,<sup>1,2,7</sup> Xueqian Zhang,<sup>2</sup> Sudarsan Rajan,<sup>1,2</sup> Karthik Mallilankaraman,<sup>1,2</sup> Rajesh Kumar Gandhirajan,<sup>1,2</sup> Ronald J. Vagnozzi,<sup>2</sup> Lucas M. Ferrer,<sup>3</sup> Krishnalatha Srekrishnanilayam,<sup>1,2</sup> Kalimuthusamy Natarajaseenivasan,<sup>1,2</sup> Sandhya Vallem,<sup>1,2</sup> Thomas Force,<sup>2,4</sup> Eric T. Choi,<sup>3,5</sup> Joseph Y. Cheung,<sup>2,4</sup> and Muniswamy Madesh<sup>1,2,\*</sup>

<sup>1</sup>Department of Biochemistry, Temple University, Philadelphia, PA 19140, USA

<sup>2</sup>Center for Translational Medicine, Temple University, Philadelphia, PA 19140, USA

<sup>3</sup>Department of Surgery, Temple University, Philadelphia, PA 19140, USA

<sup>4</sup>Department of Medicine, Temple University, Philadelphia, PA 19140, USA

<sup>5</sup>Cardiovascular Research Center, Temple University, Philadelphia, PA 19140, USA

<sup>6</sup>Stem Cell Unit and Department of Clinical Biochemistry, College of Medicine, King Khalid University, P.O. 641, 62529 Abha, Kingdom of Saudi Arabia

<sup>7</sup>These authors contributed equally to this work

\*Correspondence: [madeshm@temple.edu](mailto:madeshm@temple.edu)

<http://dx.doi.org/10.1016/j.celrep.2013.11.026>

This is an open-access article distributed under the terms of the Creative Commons Attribution License, which permits unrestricted use, distribution, and reproduction in any medium, provided the original author and source are credited.

## SUMMARY

Resting mitochondrial matrix  $\text{Ca}^{2+}$  is maintained through a mitochondrial calcium uptake 1 (MICU1)-established threshold inhibition of mitochondrial calcium uniporter (MCU) activity. It is not known how MICU1 interacts with MCU to establish this  $\text{Ca}^{2+}$  threshold for mitochondrial  $\text{Ca}^{2+}$  uptake and MCU activity. Here, we show that MICU1 localizes to the mitochondrial matrix side of the inner mitochondrial membrane and MICU1/MCU binding is determined by a MICU1 N-terminal polybasic domain and two interacting coiled-coil domains of MCU. Further investigation reveals that MICU1 forms homo-oligomers, and this oligomerization is independent of the polybasic region. However, the polybasic region confers MICU1 oligomeric binding to MCU and controls mitochondrial  $\text{Ca}^{2+}$  current ( $I_{\text{MCU}}$ ). Moreover, MICU1 EF hands regulate MCU channel activity, but do not determine MCU binding. Loss of MICU1 promotes MCU activation leading to oxidative burden and a halt to cell migration. These studies establish a molecular mechanism for MICU1 control of MCU-mediated mitochondrial  $\text{Ca}^{2+}$  accumulation, and dysregulation of this mechanism probably enhances vascular dysfunction.

## INTRODUCTION

Receptor-mediated cytosolic  $\text{Ca}^{2+}$  flooding is rapidly cleared by endoplasmic reticulum refilling, plasma membrane efflux, and mitochondrial  $\text{Ca}^{2+}$  uptake (Berridge et al., 2003; Soboloff et al., 2012). In most eukaryotic nonexcitable and excitable cells,

carriers, exchangers, and channels regulate mitochondrial  $\text{Ca}^{2+}$  uptake during the resting and active states (Drago et al., 2011; Duchen et al., 2008; Nicholls, 2005; Rizzuto et al., 2012; Santo-Domingo and Demarex, 2010; Williams et al., 2013). Following G-protein-coupled receptor or receptor-tyrosine-kinase-agonist stimulation, the mitochondrial  $\text{Ca}^{2+}$  uniporter (MCU) channel rapidly transports elevated cytosolic  $\text{Ca}^{2+}$  into the mitochondrial matrix utilizing the highly negative mitochondrial membrane potential ( $\Delta\Psi_{\text{m}}$ ) (Bernardi, 1999; Gunter et al., 1994; Kirichok et al., 2004). Mitochondrial  $\text{Ca}^{2+}$  uptake stimulates bioenergetics through activation of  $\text{Ca}^{2+}$ -sensitive dehydrogenases and thus modulates ATP synthesis (Babcock et al., 1997; Balaban, 2009; Denton and McCormack, 1980; Duchen et al., 2008; Hajnóczky et al., 1995; Hansford, 1994; McCormack et al., 1990). Reciprocally, mitochondrial  $\text{Ca}^{2+}$  overload promotes physical damage to mitochondria leading to bioenergetic crisis and cell death (Orrenius et al., 2003; Szalai et al., 1999). Pathophysiological dysregulation of mitochondrial  $\text{Ca}^{2+}$  uptake has been linked to organ damage via chronic oxidative burden, autophagy, and cellular dysfunction (Baines et al., 2005; Cárdenas et al., 2010; Clapham, 2007; Joiner et al., 2012; Lemasters et al., 2009; Mallilankaraman et al., 2012b).

Mitochondrial  $\text{Ca}^{2+}$  uptake has been functionally described for decades, but only recently using integrative bioinformatics and RNAi screening approaches, three components of the MCU complex (mitochondrial calcium uptake 1 [MICU1], MCU, and MCU regulator 1) were identified that together constitute the activity of MCU (Baughman et al., 2011; De Stefani et al., 2011; Mallilankaraman et al., 2012a, b; Perocchi et al., 2010). Although the mitochondrial uniporter complex tightly regulates  $\text{Ca}^{2+}$  influx, the molecular mechanisms of uniporter regulation are unclear. This unknown regulatory mechanism stems from the observation that mitochondrial  $\text{Ca}^{2+}$  influx exhibits a finite trigger proposed as a “set point” in 1978 (Nicholls, 1978, 2005). The set point is overcome and the mitochondria begins  $\text{Ca}^{2+}$  uptake at cytosolic  $\text{Ca}^{2+}$  levels exceeding  $\sim 3 \mu\text{M}$ . The trigger was characterized as the function

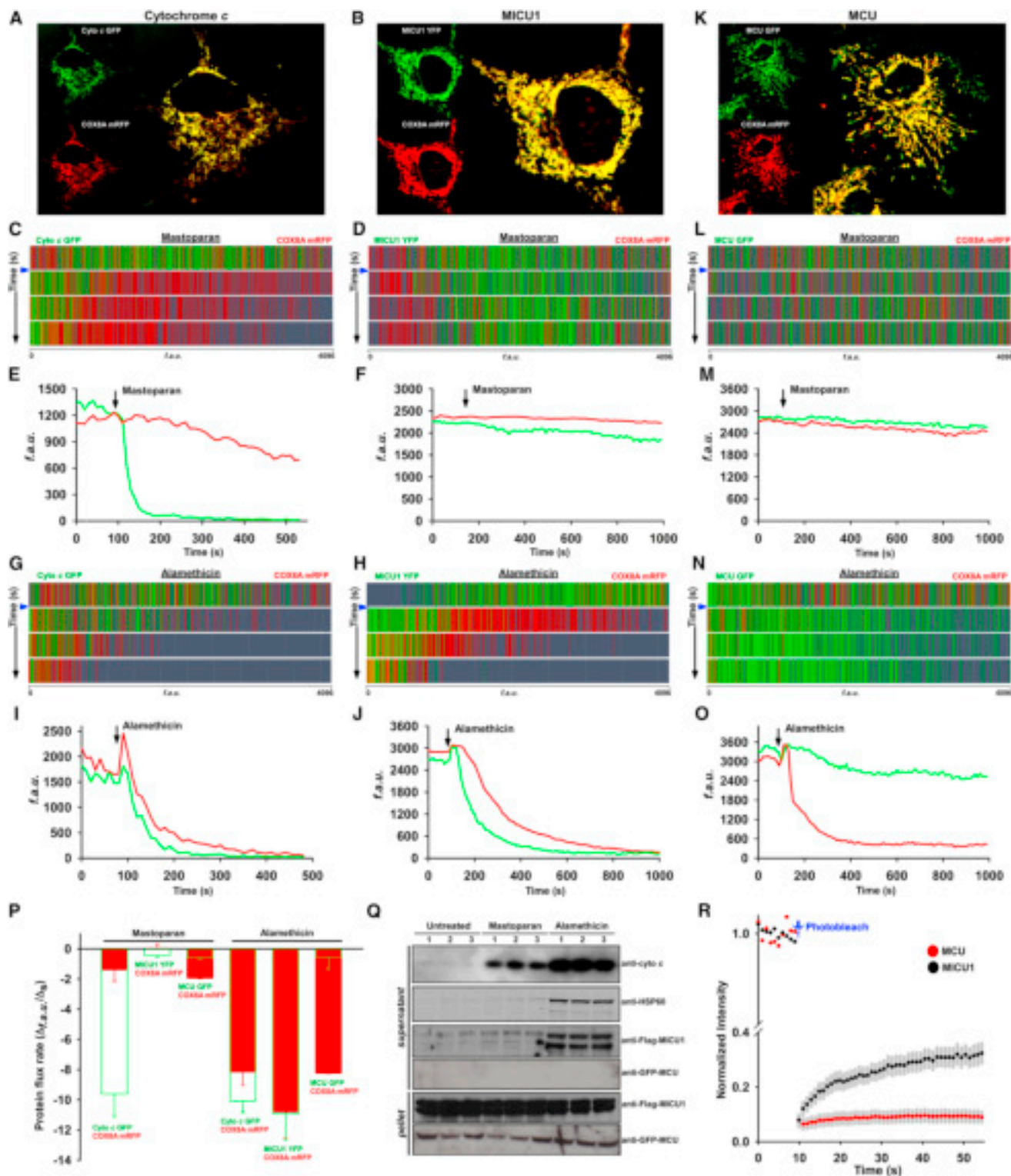


**Figure 1. Protein Flux Dynamics Illustrate MICU1 Is Localized in the Mitochondrial Matrix Compartment**

(A) HeLa cells were cotransfected with cytochrome c-GFP and COX8A-mRFP (MTS) plasmid constructs.

(B) Similarly, HeLa cells were cotransfected with MICU1-YFP and COX8-mRFP (MTS).

(C and D) Plasma membranes of HeLa cells were briefly permeabilized with digitonin (0.002% w/v) containing intracellular medium for 7 min. Cells were treated with mastoparan (20  $\mu$ g/ml) to trigger outer mitochondrial membrane permeabilization. Protein flux dynamics were visualized using confocal microscopy. The

(legend continued on next page)

of MCU-associated protein MICU1 which is able to suppress mitochondrial  $\text{Ca}^{2+}$  uptake up to the cytosolic levels  $\sim 3 \mu\text{M Ca}^{2+}$  (Mallilankaraman et al., 2012b). Thus far, MICU1 is the only known protein that interacts with MCU to prevent mitochondrial  $\text{Ca}^{2+}$  uptake under resting conditions (Mallilankaraman et al., 2012b), but the MICU1 localization and the binding domains of the MICU1/MCU complex that establish the set point are unknown.

Here, we show that MICU1 interacts with MCU in the mitochondrial matrix and MICU1/MCU binding is determined by a MICU1 N-terminal polybasic domain and two coiled-coil MCU domains. MICU1 EF hands regulate MCU channel activity, but not MICU1/MCU binding. Additionally, loss of MICU1 induces MCU activity leading to vascular endothelial oxidative stress and diminished endothelial cell migration.

## RESULTS

### Protein Flux Analysis Establishes MICU1 Is Compartmentalized in the Mitochondrial Matrix

The MCU pore subunit is located in the inner mitochondrial membrane (IMM), and thus its regulator, MICU1, must be present either in the intermembrane space or the matrix side of the mitochondrial inner membrane. To determine the suborganelle localization of MICU1, we developed a dynamic protein flux assay using confocal microscopy in which the outer mitochondrial membrane (OMM) or both the OMM and IMM of the mitochondria were selectively permeabilized and release of MICU1 was subsequently visualized from the mitochondrial compartments. HeLa cells were cotransfected with expression vector pairs encoding yellow fluorescent protein (YFP)-tagged MICU1 and monomeric red fluorescent protein (mRFP)-tagged mitochondrial targeting sequence of matrix-localized cytochrome *c* oxidase subunit 8 (COX8) (Figure 1B) or mitochondrial intermembrane space protein, GFP-tagged cytochrome *c* (cyto *c*) cotransfected with mRFP-COX8 (Figure 1A). Combinations of both cyto *c*/COX8 and MICU1/COX8 showed general mitochondrial localization (Figures 1A and 1B). To visualize the MICU1 compartmentalization, the plasma membrane was permeabilized using 0.002% digitonin (20  $\mu\text{g/ml}$ ) and permeabilized cells were bathed in digitonin-free intracellular medium (ICM) before exposure to mitochondrial permeabilizing agents.

The cyto *c*/COX8 cotransfected permeabilized cells were subjected to mastoparan (20  $\mu\text{g/ml}$ ), a wasp venom peptide toxin

that induces OMM permeabilization (Kluck et al., 1999; Pfeiffer et al., 1995). The release of intermembrane-space-resident proteins due to mastoparan was visualized by confocal microscopy in real time. OMM permeabilization by mastoparan rapidly released cyto *c*, but not matrix-localized COX8 (Figures 1C and 1E). Similarly, MICU1-YFP/COX8-mRFP permeabilized cells were exposed to mastoparan. We found that mitochondrial localized MICU1 and COX8 were not released from the mitochondrial intermembrane space (Figures 1D and 1F). We next asked whether permeabilization of both the OMM and the IMM promotes MICU1 release from the mitochondrial matrix. Permeabilized cells were exposed to a fungal peptide, alamethicin (20  $\mu\text{g/ml}$ ), that induces large pores in both mitochondrial membranes (Kluck et al., 1999). Permeabilization of both membranes induced the release of COX8 from the matrix in addition to cyto *c* from the intermembrane space (Figures 1G, 1I, and 1P). It has been recently reported that MICU1 exists in the intermembrane space (Csordás et al., 2013), but similar to COX8, MICU1 was released only upon permeabilization of both the OMM and IMM by alamethicin (Figures 1H, 1J, and 1P). The integral inner membrane channel pore subunit MCU was not released by mastoparan or alamethicin permeabilization (Figures 1K–1P). The dynamic protein flux assay was complemented by western blot analysis. As expected, cyto *c* was released by both mastoparan and alamethicin and appeared in the cytosolic supernatant (Figure 1Q). MICU1 was only released by alamethicin, whereas integral membrane MCU was not released by either mastoparan or alamethicin (Figure 1Q). A soluble mitochondrial matrix protein heat shock protein 60 (HSP60) was used as a substitute for COX8 (Figure 1Q). Further, we examined whether MCU and MICU1 diffuse rapidly after photobleaching. Photobleaching of MICU1, but not MCU, showed rapid fluorescence recovery after photobleaching (FRAP). This result suggested that MICU1 is less associated with the IMM than MCU (Figure 1R). These results reveal that MICU1 is compartmentalized in the mitochondrial matrix side of the IMM.

### Mapping of MICU1- and MCU-Binding Regions Reveals Conserved MICU1 Polybasic Motif Domains, but Not EF Hand Domains, Are Essential for MCU Binding

Although MICU1 and MCU form a complex (Mallilankaraman et al., 2012b; Perocchi et al., 2010), it is not known which regions of MICU1 and MCU determine binding. To map the binding

depletion of either cyto *c*-GFP or MICU1-YFP was depicted as representative green histogram lines from an individual experiment. The depletion of COX8A-mRFP was depicted as representative red histogram lines from the same individual experiment. Each row corresponds to different time intervals before (top row) and after (bottom three rows) mastoparan challenge (indicated by blue arrow).  $n = 6-9$ . f.a.u., fluorescence arbitrary units.

(E) Representative protein release traces from (C) of cytochrome *c* (green) and COX8A (red) following mastoparan.  $n = 6-9$ .

(F) Representative protein release traces from (D) of MICU1 (green) and COX8A (red) following mastoparan.  $n = 6-9$ .

(G and H) Release illustration of cytochrome *c* and COX8A or MICU1 and COX8A flux dynamics before (top row) and after (bottom three rows) alamethicin (20  $\mu\text{g/ml}$ ) addition (indicated by blue arrow).  $n = 6-9$ .

(I and J) Representative traces from (G) and (H) of cytochrome *c* and COX8A or MICU1 and COX8A depletion before and after alamethicin addition.  $n = 6-9$ .

(K–O) Similar to cytochrome *c* and MICU1, MCU-GFP flux assessment was performed.  $n = 6-9$ .

(P) Dissipation of fluorescence intensity was calculated as flux rate after mastoparan or alamethicin addition. Mean  $\pm$  SEM;  $n = 6-9$ .

(Q) To assess the localization of MICU1, HeLa cells were permeabilized and exposed to mastoparan or alamethicin (20  $\mu\text{g/ml}$ ) for 5 min. Cytosolic (supernatant) and mitochondrial (pellet) fractions were subjected to immunoblotting to examine the release of cytochrome *c* (intermembrane space marker), HSP60 (matrix marker), MICU1-Flag, and MCU-GFP from mitochondria. Lanes 1, 2, and 3 refer to triplicate samples.  $n = 3$ .

(R) Time course of FRAP from cells expressing MICU1-YFP or MCU-GFP. The FRAP recovery curve is a plot of the normalized fluorescence recovery versus time. Mean  $\pm$  SEM;  $n = 6$ .

regions of MICU1 and MCU, we generated five hemagglutinin (HA)-tagged MICU1 truncation mutants (Figure 2A) and transfected these into COS-7 cells stably expressing GFP-tagged full-length MCU. The transfected cell lysates were subjected to immunoprecipitation and western blot analysis. Immunoprecipitation of GFP-tagged MCU pulled down all MICU1 truncation mutants except deletion of amino acids 131–200 (MICU1- $\Delta$ 2) (Figure 2B). Intriguingly, the MICU1- $\Delta$ 1 (deletion of amino acids 61–130) partially interacts with wild-type MCU (Figure 2B). Although the effect of the MICU1- $\Delta$ 2 deletion was profound, lack of any interaction suggests a conformational deformity of MICU1- $\Delta$ 2 as a result of the truncation. In contrast, the partial interaction of MICU1- $\Delta$ 1 suggests that the protein is maintaining an interacting tertiary structure that is recognized by MCU. Therefore, we examined the MICU1- $\Delta$ 1 amino acid sequence for evolutionarily conserved interaction motifs and found a series of positively charged lysine residues (amino acids [aa] 99–110) (Figures S1A and S1B) which corresponds to the consensus sequence of a polybasic region motif which is known as not only an interaction motif but also as a membrane-anchoring motif (Hancock et al., 1990; Heo et al., 2006; Papayannopoulos et al., 2005; Williams, 2003). The polybasic N-terminal region domain was mutated to polyglutamine (MICU1- $\Delta$ K) (Figure 2C), and MICU1- $\Delta$ K reduced MCU interactions (Figure 2D); however, MICU1- $\Delta$ K still localized to the mitochondria (Figures S1D and S1E). The marked, but not complete, loss of interaction with MCU suggests the MICU1 polybasic region motif is a determinant of MICU1/MCU interaction. The profound loss of binding in MICU1- $\Delta$ 2 may be a consequence of the deleted region's proximity to an EF hand of MICU1. To determine if the EF hands are necessary for MCU binding, both EF hands were mutated (Figure 2C). Although functionally important (Mallilankaraman et al., 2012b; Perocchi et al., 2010), the EF hands of MICU1 did not determine MCU binding (Figure 2D). This result also demonstrates that although MICU1- $\Delta$ K has functional EF hands, it failed to interact with MCU (Figure 2D). We next asked whether EF hands'  $\text{Ca}^{2+}$  binding domains may participate in MCU/MICU1 binding. We therefore tested whether  $\text{Ca}^{2+}$  determines MICU1/MCU binding using MICU1 full-length and single and double EF1 and EF2 mutants. Our coimmunoprecipitation data demonstrated that MICU1/MCU binding is independent of  $[\text{Ca}^{2+}]$  (Figure 2E). Together, these results indicate that the polybasic region, but not the EF hands of MICU1, are determinant of MCU binding.

### MCU Coiled-Coil Domains Are Determinants of MICU1 Binding

Next to map which regions of MCU bind MICU1, we created three MCU truncation mutants stably expressing in COS-7 cells that were lacking aa 150–220 (MCU- $\Delta$ 1), aa 291–320 (MCU- $\Delta$ 2), or aa 321–351 (MCU- $\Delta$ 3; Figure 3A). Then, these stable cells were transfected with full-length MICU1-HA plasmid constructs. The pull-down of full-length MICU1-HA was unable to immunoprecipitate MCU- $\Delta$ 1 and MCU- $\Delta$ 3 suggesting that these regions corresponding to MCU coiled-coil domains are essential for MICU1 binding (Figures 3B and S1C). To validate the coimmunoprecipitation data, we performed fluorescence resonance energy transfer (FRET) acceptor photobleaching to determine

whether MCU- $\Delta$ 1 and - $\Delta$ 3 interact with MICU1. Coexpression of mitochondrial marker COX8A-mRFP and MCU-GFP constructs revealed that MCU  $\Delta$ 1,  $\Delta$ 2, and  $\Delta$ 3 mutants did not alter the mitochondrial targeting (Figure S2). Comparable protein expressions of wild-type,  $\Delta$ 1,  $\Delta$ 2, and  $\Delta$ 3 MCU-GFP were selected for FRET analysis. Expectedly, MCU-GFP and MICU1-YFP interact; however, neither MCU-GFP nor MICU1-YFP interact with matrix-localized COX8A-RFP (Figures 3C–3E). Similar to coimmunoprecipitation analysis, MCU wild-type and MCU- $\Delta$ 2, but not MCU- $\Delta$ 1 and MCU- $\Delta$ 3, interact with MICU1 (Figures 3C and 3F–3H). Further, we have also conducted interaction studies by yeast two-hybrid assay (Figure 3I). In support of coimmunoprecipitation and FRET, MCU wild-type and MCU- $\Delta$ 2 showed positive blue colonies, but MCU- $\Delta$ 1 and MCU- $\Delta$ 3 did not, indicating that MCU wild-type and MCU- $\Delta$ 2 interact with MICU1 (Figure 3J). Collectively, these results demonstrate that MCU- $\Delta$ 1 and MCU- $\Delta$ 3, regions corresponding to the coiled-coil domains, are necessary for interaction with MICU1.

### MICU1 Polybasic Region and EF Hands Regulate MCU-Mediated Mitochondrial $\text{Ca}^{2+}$ Uptake

We next sought to characterize whether MICU1 undergoes oligomerization as a mechanistic step in regulation of MCU-mediated  $\text{Ca}^{2+}$  uptake. To evaluate the possibility of MICU1 oligomerization, we developed a coimmunoprecipitation strategy using cotransfection of two MICU1 constructs (MICU1-HA and MICU1-Flag) in COS-7 cells. Coimmunoprecipitation of MICU1-Flag with HA antibody indicated that MICU1-HA and MICU1-Flag are able to form oligomeric complexes (Figure 4A, right panel). Similarly, COS-7 cells were cotransfected with MICU1-Flag and MICU1- $\Delta$ K-YFP plasmid constructs. Coimmunoprecipitation of MICU1-Flag with GFP antibody indicated that MICU1-Flag is still able to oligomerize with MICU1- $\Delta$ K (Figure 4B, right panel). These results demonstrate that the polybasic region of MICU1 is not a MICU1/MICU1 interaction domain but instead supports the polybasic region's role in MCU interaction.

Having determined the binding regions of MCU and MICU1 through a series of deletion and mutation analysis, we next asked whether MICU1- $\Delta$ K and MICU1- $\Delta$ EF1 $\Delta$ EF2 affect MCU-mediated  $[\text{Ca}^{2+}]_m$  uptake. Permeabilized control, MICU1- $\Delta$ K, and MICU1- $\Delta$ EF1 $\Delta$ EF2-expressing HeLa cells were loaded with Fura-FF to determine  $[\text{Ca}^{2+}]_m$  uptake rate as a decay of extramitochondrial  $\text{Ca}^{2+}$  and JC-1 to simultaneously monitor mitochondrial membrane potential ( $\Delta\Psi_m$ ) dynamics. MICU1 actively inhibits MCU at cytosolic  $\text{Ca}^{2+}$  levels  $<3 \mu\text{M}$  (Mallilankaraman et al., 2012b). Therefore, to determine the phenotype of the MICU1- $\Delta$ K, HeLa cells were challenged with a  $1 \mu\text{M}$   $\text{Ca}^{2+}$  bolus, well within the functional inhibitory range of wild-type MICU1. We found that MICU1- $\Delta$ K cells rapidly cleared the  $1 \mu\text{M}$   $\text{Ca}^{2+}$  bolus under normal  $\Delta\Psi_m$  indicating the loss of MICU1 inhibition of MCU activity at  $<3 \mu\text{M}$ . Conversely, control cells did not exhibit MCU-dependent  $\text{Ca}^{2+}$  uptake (Figures 4C–4F), because the MICU1 inhibition was intact. Next, we examined the total amount of  $\text{Ca}^{2+}$  buffered by control and MICU1- $\Delta$ K mitochondria using the mitochondrial uncoupler, CCCP. MICU1- $\Delta$ K-overexpressing cells accumulated large amounts of  $\text{Ca}^{2+}$  (Figure 4G) suggesting that MICU1- $\Delta$ K is unable to properly interact with MCU to establish the set point for MCU-mediated  $\text{Ca}^{2+}$  uptake. Functionally,

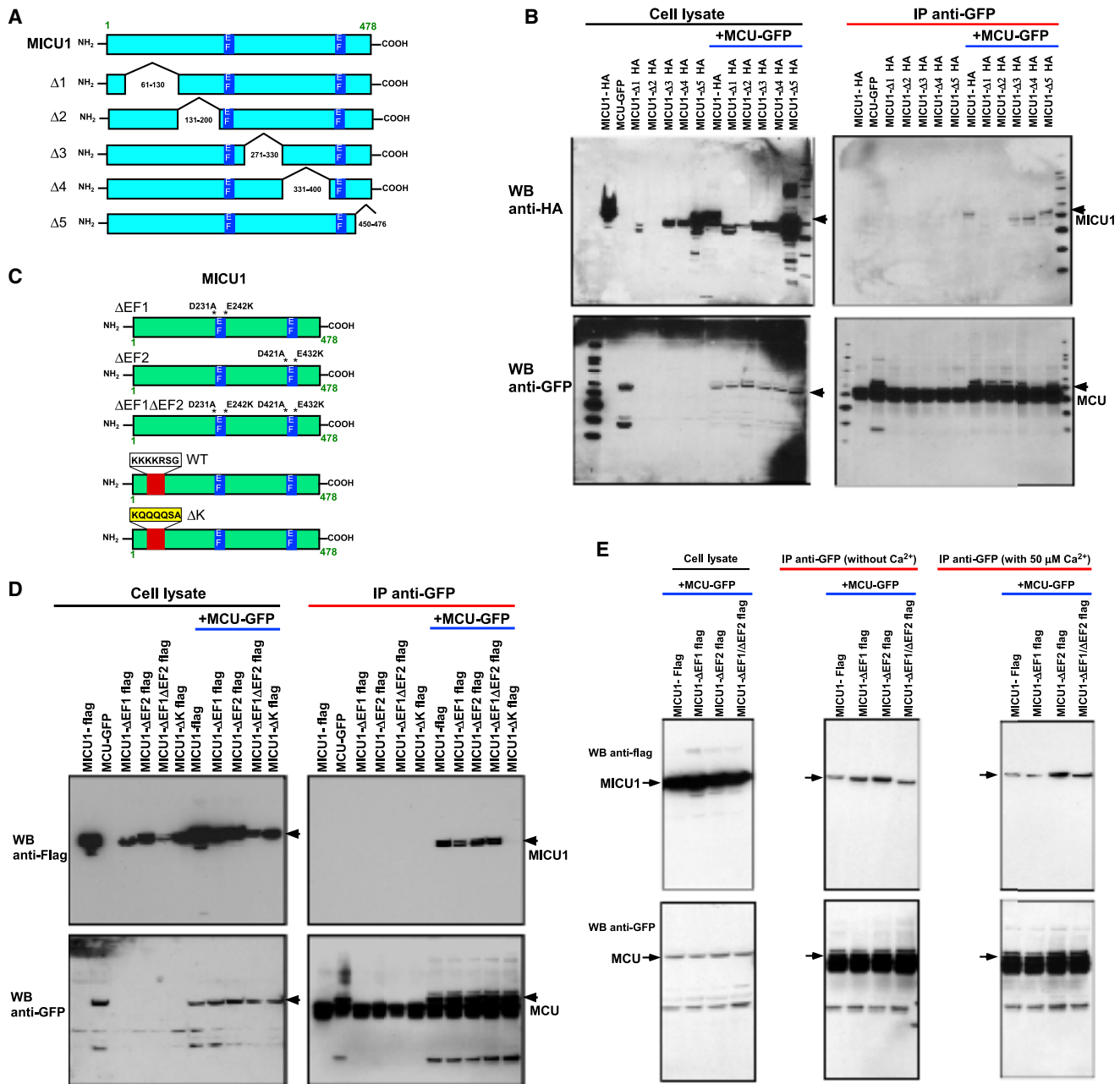


**Figure 2. Mapping the MICU1 Interaction Domains with MCU**

(A) Scheme depicts full-length MICU1 and truncation constructs.

(B) Stably MCU-GFP-expressing COS-7 cells were transfected with HA-tagged full-length MICU1 or truncations. Following immunoprecipitation with GFP antibody, total cell lysates and immunoprecipitated materials were subjected to western blot analysis. Cell lysates were probed with HA (top left) or GFP (bottom left) antibodies to serve as inputs. Immunoprecipitated samples were probed with HA (top right) or GFP (bottom right) antibodies. GFP antibodies coimmunoprecipitate full-length MICU1, Δ3, Δ4, and Δ5 MICU1-HA truncations, but not MICU1-Δ1 and MICU1-Δ2. n = 3–5. IP, immunoprecipitation; WB, western blot.

(C) Scheme depicts full-length MICU1 and MICU1-ΔEF1, MICU1-ΔEF2, MICU1-ΔEF1ΔEF2, and MICU1-ΔK mutant constructs. WT, wild-type.

(D) Stably MCU-GFP-expressing COS-7 cells were transfected with Flag-tagged full-length MICU1 and mutants. Following immunoprecipitation with GFP antibody, total cell lysates and immunoprecipitated materials were subjected to western blot analysis. Cell lysates were probed with Flag (top left) or GFP (bottom left) antibodies to serve as inputs. Immunoprecipitated samples were probed with Flag (top right) or GFP (bottom right) antibodies. GFP antibodies coimmunoprecipitate full-length MICU1, MICU1-ΔEF1, MICU1-ΔEF2, and MICU1-ΔEF1ΔEF2, but not MICU1-ΔK mutant. n = 3.

(E) As described in (D), stably MCU-GFP-expressing COS-7 cells were transfected with Flag-tagged MICU1-ΔEF1, MICU1-ΔEF2, and MICU1-ΔEF1ΔEF2 mutants. Cell lysates were incubated with or without 50 μM Ca<sup>2+</sup>, immunoprecipitation was performed with GFP antibody, and cell lysates were subjected to western blot analysis. Cell lysates were probed with Flag (top left) or GFP (bottom left) antibodies to serve as inputs. Immunoprecipitated samples were probed with Flag (top middle and right) or GFP antibodies (bottom middle and right).

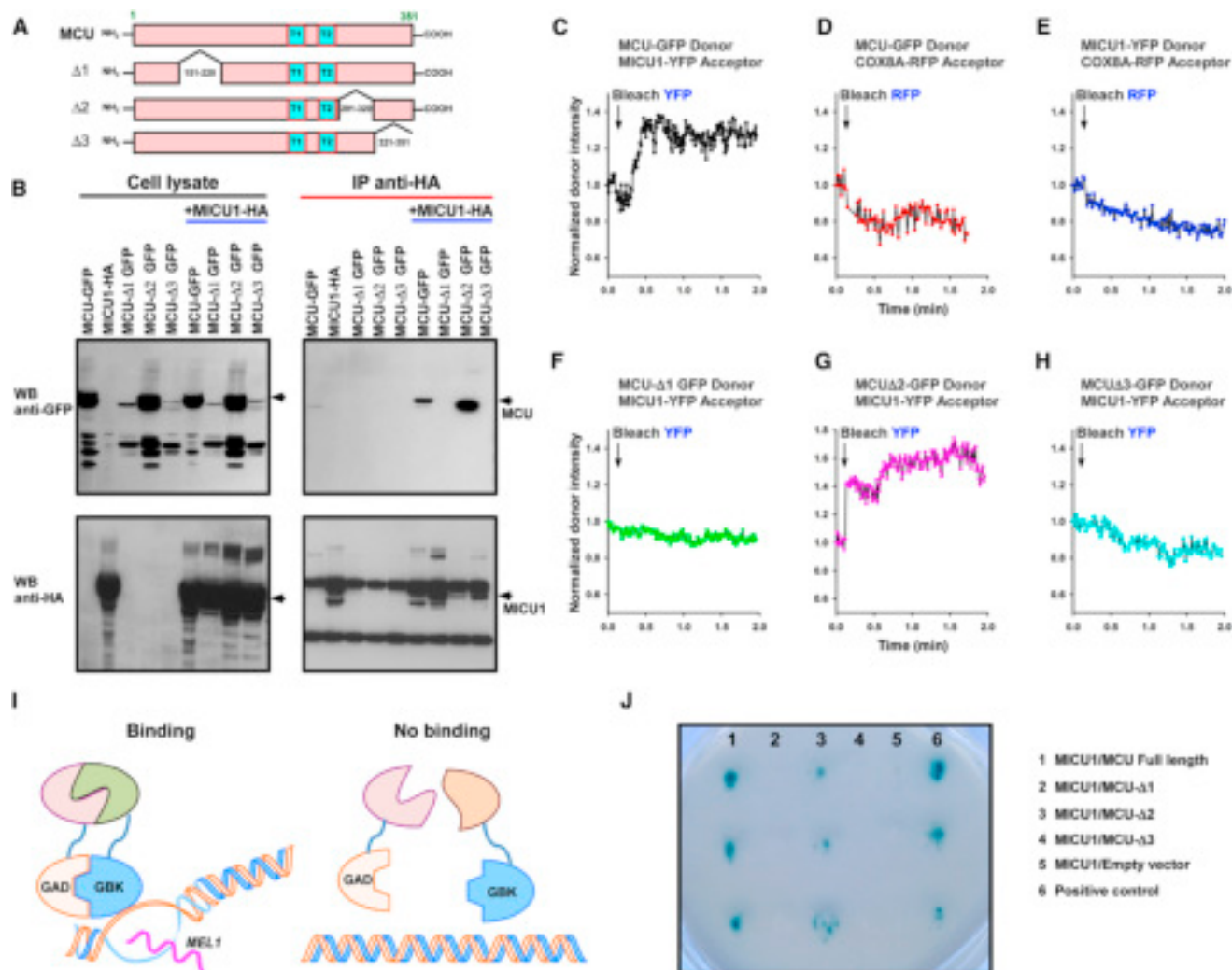


**Figure 3. MCU Coiled-Coil Domains Are Determinant of MICU1 Binding**

(A) Scheme depicts full-length MCU and truncation constructs.

(B) Stably MICU1-HA expressing COS-7 cells were transfected with GFP-tagged full-length MCU or truncations. Following immunoprecipitation with HA antibody, total cell lysates and immunoprecipitated materials were subjected to western blot analysis. Ten percent of cell lysates were probed with GFP (top left) or HA antibodies (bottom left) to serve as inputs. Immunoprecipitated samples were probed with GFP (top right) or HA antibodies (bottom right). HA antibodies coimmunoprecipitate full-length MCU and MCU-Δ2, but not MCU-Δ1 and MCU-Δ3. n = 3.

(C) HeLa cells were cotransfected with MCU-GFP donor and MICU1-YFP acceptor. MICU1-YFP acceptor was bleached, and a representative trace of the MCU-GFP donor fluorescence is shown. n = 4.

(D) Similarly, MCU-GFP donor and COX8A-RFP acceptor. n = 4.

(E) MICU1-YFP donor and COX8A-RFP acceptor. n = 4.

(F) MCUΔ1-GFP donor and MICU1-YFP acceptor. n = 3.

(G) MCUΔ2-GFP donor and MICU1-YFP acceptor. n = 3.

(H) MCUΔ3-GFP donor and MICU1-YFP acceptor. n = 3.

(I) Scheme depicts yeast two-hybrid system for analysis of MCU and MICU1 binding.

(J) Full-length MCU; MCU-Δ1, MCU-Δ2, or MCU-Δ3; and MICU1 were subcloned into pGBKT7 and pGADT7 vectors as bait and prey, respectively. After transformation, screening was performed by stringent selection (growth on quadruple dropout medium and resistance to the antibiotic aureobasidin A) and blue colonies confirmed the MICU1/MCU interaction. Each column represents triplicates of MICU1/MCU, MICU1/MCU-Δ1, MICU1/MCU-Δ2, MICU1/MCU-Δ3, MICU1/empty vector, and a positive control from the manufacturer (from left to right). n = 3.

MICU1 EF hands are the  $\text{Ca}^{2+}$  sensor of the MCU complex, and although EF hand mutants bind MCU (Figure 2D), the mutations of EF1, EF2, or EF1/EF2 (Figure 2C) led to dysfunction with a functional phenotype similar to MICU1 knockdown (KD) (Malli-

lankaraman et al., 2012b) in which the mitochondria constitutively accumulate  $\text{Ca}^{2+}$  that would otherwise remain as cytosolic  $\text{Ca}^{2+}$  (Figures 4H–4L). These data indicate that both polybasic and EF hands are essential for MICU1 regulation of MCU.

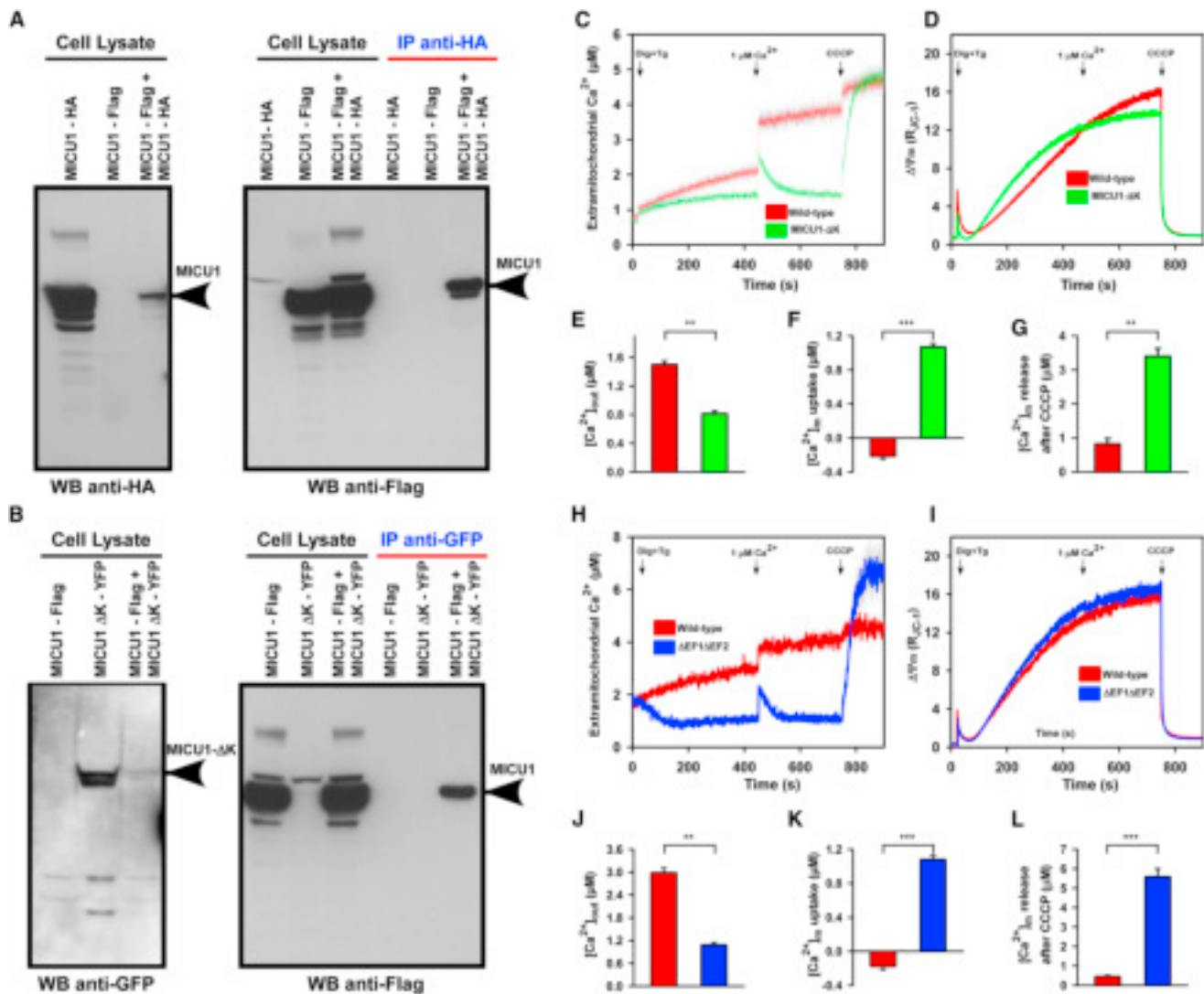


**Figure 4. MICU1 Binding and Functional Domains Regulate MCU-Mediated  $Ca^{2+}$  Uptake**

(A) COS-7 wild-type cells were cotransfected with HA-tagged full-length MICU1 and Flag-tagged full-length MICU1 plasmid constructs. Following immunoprecipitation with HA antibody, total cell lysates and immunoprecipitated materials were subjected to western blot analysis. Cell lysates were probed with HA (left) or Flag antibodies (right panel, first three lanes) to serve as inputs. Immunoprecipitated samples were probed with Flag (right panel, last three lanes).  $n = 3$ .

(B) COS-7 wild-type cells were cotransfected with Flag-tagged full-length MICU1 and YFP-tagged MICU1-ΔK plasmid constructs. Following immunoprecipitation with GFP antibody, total cell lysates and immunoprecipitated materials were subjected to western blot analysis. Cell lysates were probed with GFP (left) or Flag (right panel, first three lanes) antibodies to serve as inputs. Immunoprecipitated samples were probed with anti-Flag (right panel, last three lanes).  $n = 3$ .

(C and D) HeLa cells were transfected with MICU1-ΔK plasmid, and stable cells were generated after G418 selection. MICU1-ΔK and wild-type cells were permeabilized with 0.004% digitonin in ICM buffer and loaded with extramitochondrial ratiometric  $Ca^{2+}$  indicator Fura-2FF. These cells were also loaded with ratiometric  $\Delta\Psi_m$  indicator JC-1. Cells were then challenged with  $1 \mu M Ca^{2+}$  bolus. Finally, total mitochondrial  $Ca^{2+}$  uptake and  $\Delta\Psi_m$  dissipation were determined by uncoupler CCCP. Mean  $\pm$  SEM;  $n = 3-6$ .

(E) Quantitation of wild-type and MICU1-ΔK extramitochondrial  $[Ca^{2+}]_{out}$  (to 450 s). Mean  $\pm$  SEM; \*\* $p < 0.01$ ;  $n = 3-6$ .

(F) Quantitation of  $1 \mu M Ca^{2+}$  bolus uptake,  $[Ca^{2+}]_m$ . Mean  $\pm$  SEM; \*\*\* $p < 0.001$ ,  $n = 3-6$ .

(G) Quantitation of mitochondrial  $Ca^{2+}$  release following CCCP. Mean  $\pm$  SEM; \*\* $p < 0.01$ ,  $n = 3-6$ .

(H-L) Similar to MICU1-ΔK, EF hand double-mutant  $\Delta EF1\Delta EF2$  was assessed for MCU-mediated  $Ca^{2+}$  uptake and  $\Delta\Psi_m$  dynamics. Mean  $\pm$  SEM; \*\* $p < 0.01$ , \*\*\* $p < 0.001$ ,  $n = 3-6$ .

#### MICU1 Polybasic and EF Hand Motifs Regulate $I_{MCU}$

Because MCU-mediated mitochondrial  $Ca^{2+}$  uptake is regulated by MICU1, we examined whether MICU1-ΔK or MICU1-ΔEF1ΔEF2 mutants were able to regulate MCU current ( $I_{MCU}$ )

in HeLa cells. To measure  $I_{MCU}$ , we utilized mitoplast patch-clamp (Chaudhuri et al., 2013; Fieni et al., 2012; Joiner et al., 2012; Kirichok et al., 2004). As a first step, freshly isolated mitochondria were loaded with  $\Delta\Psi_m$  indicator, rhodamine 123, and

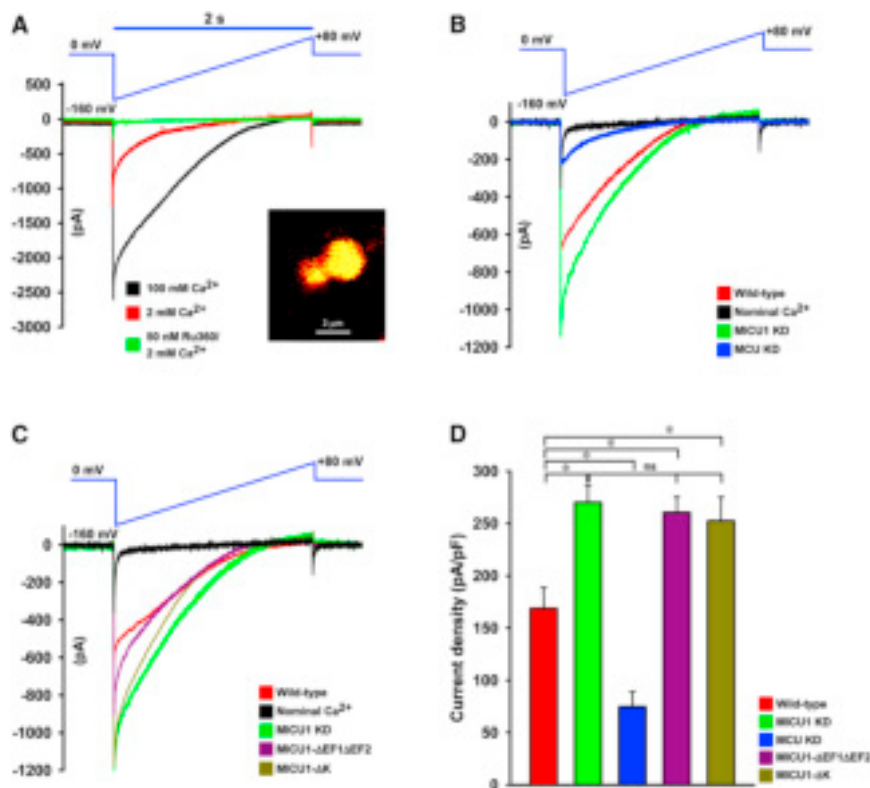


**Figure 5. MICU1 Polybasic and EF Hand Domains Regulate  $I_{MCU}$**

(A) Mitoplasts generated from HeLa mitochondria were loaded with  $\Delta\Psi_m$  indicator rhodamine 123 and visualized using confocal microscopy (inset). Mitoplast current ( $I_{MCU}$ ) was recorded before and after application of 2 (red) or 100 mM (black)  $Ca^{2+}$  to the bath medium. Currents were measured during a voltage ramp as indicated.  $I_{MCU}$  recorded in the presence of 2 mM  $Ca^{2+}$  was nearly completely inhibited by 50 nM of Ru360 (green trace). Traces are a representative single recording of  $I_{MCU}$ .  $n = 6$ .

(B) Mitoplasts generated from HeLa wild-type cells (red), stable MICU1 KD (green), or stable MCU KD (blue) were used for  $I_{MCU}$  measurements.  $I_{MCU}$  was measured using 5 mM bath  $Ca^{2+}$  unless otherwise indicated. Nominal  $Ca^{2+}$ -free buffer (no EGTA; contaminant  $Ca^{2+} \sim 6 \mu M$ ) was used as a control and trace shown in black. Traces are a representative single recording of  $I_{MCU}$ .  $n = 6-12$ .

(C) Similarly,  $I_{MCU}$  from MICU1 mutants MICU1- $\Delta EF1\Delta EF2$  (purple) and MICU1- $\Delta K$  (brown) mitoplasts were measured and compared to wild-type (red) and MICU1 KD (green).  $I_{MCU}$  was measured with 5 mM bath  $Ca^{2+}$  except for nominal  $Ca^{2+}$ -free (black) medium. Traces are a representative single recording of  $I_{MCU}$ .  $n = 6-12$ .

(D)  $I_{MCU}$  densities (pA/pF) for wild-type (red), MICU1KD (green), MCU KD (blue), MICU1- $\Delta EF1\Delta EF2$  (purple), and MICU1- $\Delta K$  (brown). Mean  $\pm$  SEM; \* $p < 0.05$ ; ns, not significant,  $n = 6-12$ .

the mitoplast preparation was confirmed by confocal imaging (Figure 5A, inset). In the patch-clamp of whole-mitoplast configuration, the addition of 2 mM  $Ca^{2+}$  to the bath elicited an inwardly rectifying  $Ca^{2+}$  current that is almost completely blocked by 50 nM Ru360 (Kirichok et al., 2004; Figure 5A). Next, we examined if knockdown of human MICU1 or MCU proteins altered  $I_{MCU}$ . Compared to control conditions,  $I_{MCU}$  in mitoplasts from MCU knockdown (MCU KD) cells was significantly lower (Figures 5B and 5D) which is correlated with MCU-mediated  $Ca^{2+}$  uptake (Figures S3A-S3C). In sharp contrast, stable knockdown of MICU1 exhibited larger  $I_{MCU}$  (Figures 5B and 5D). Finally, we conducted mitoplast patch-clamp recordings in MICU1- $\Delta K$  and MICU1- $\Delta EF1\Delta EF2$  mutants overexpressing HeLa cells. The electrophysiology revealed that MICU1- $\Delta K$  and  $\Delta EF1\Delta EF2$  mitoplasts exhibited larger MCU current densities when compared to MCU currents from wild-type (Figures 5C and 5D). Having demonstrated the MCU  $\Delta 1$  and  $\Delta 3$  role in MICU1 binding, we next tested whether deletion of coiled-coil domains alter  $I_{MCU}$ . MCU number 861 small hairpin RNA (shRNA)-insensitive MCU full-length and mutant constructs were stably expressed in MCU KD HeLa cells, and  $I_{MCU}$  was measured (Figures S3D-S3F). Reconstitution of full-length MCU in MCU KD mitoplasts re-established  $I_{MCU}$  (Figures S3E and S3F). Interestingly, MCU- $\Delta 1$  and MCU- $\Delta 3$  generated larger  $I_{MCU}$  than MCU- $\Delta 2$  indicating that MCU- $\Delta 1$  and - $\Delta 3$  regions are necessary for MICU1-mediated regulation of MCU activity. Taken together, these data strongly support that loss of MICU1 polybasic or EF hands increase the  $I_{MCU}$ , exhibiting dominant negative phenotypes.

### Loss of MICU1 Promotes Mitochondrial $Ca^{2+}$ Accumulation and Oxidative Burden, Halting Endothelial Cell Migration

The ability of MICU1 to suppress MCU-mediated basal mitochondrial  $Ca^{2+}$  accumulation suggests that MICU1, rather than the MCU pore, is sensing  $Ca^{2+}$  uptake from the cytosol (Mallikarayanan et al., 2012b). Ablation of MICU1 causes mitochondrial  $Ca^{2+}$ -dependent chronic oxidant elevation and cellular stress. The MICU1 and MCU expression profiles in cell lines and primary cells indicated that human aortic endothelial cells have relatively high levels of MICU1 mRNA when compared to other cell types (Figures S4A and S4B; Aichberger et al., 2005). Nevertheless, MCU mRNA levels were relatively unchanged (Figures S4A and S4B). Therefore, we tested whether MICU1 downregulation impacts pathophysiological endothelial cell (EC) function. Because EC function is compromised in various cardiovascular disease states (Libby et al., 2006), we performed quantitative RT-PCR (qRT-PCR) to assess MICU1 expression in human control and cardiovascular disease (CVD)-derived primary ECs (Table S1). MICU1, but not MCU, mRNA levels were markedly downregulated in CVD ECs (Figure 6A). Basal  $[Ca^{2+}]_m$  was considerably elevated in ECs derived from CVD patients when compared to control ECs. Further, reconstitution of MICU1 in CVD ECs reduced the  $[Ca^{2+}]_m$  accumulation (Figures 6B and 6C). These results were further confirmed by the reduction of MICU1 protein in patients (Figure 6D). To examine if loss of MICU1 led to more MCU activity, mitochondria were isolated and mitoplast patch-clamp was performed. CVD ECs exhibited

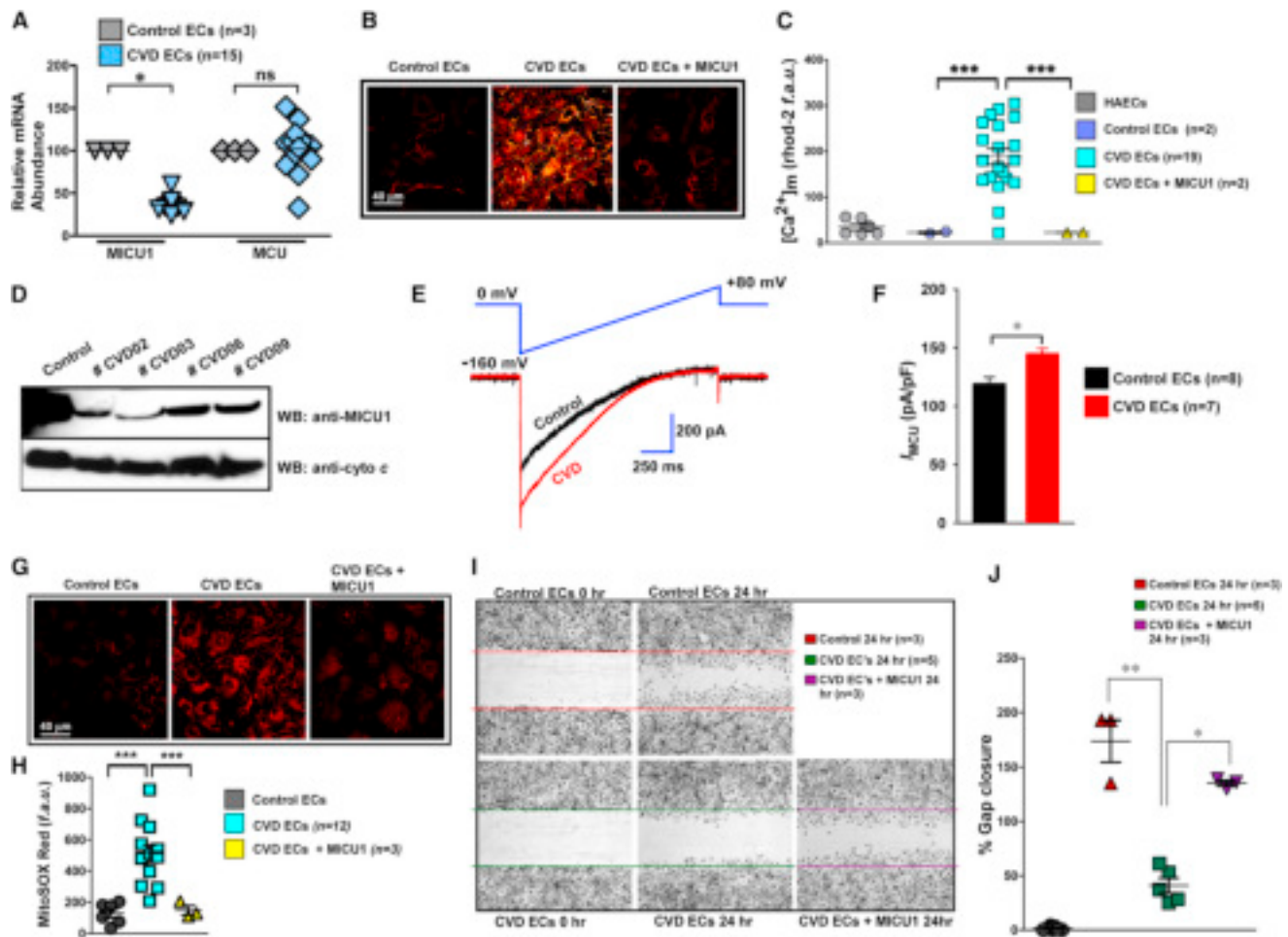


**Figure 6. Loss of MICU1 Exacerbates MCU-Mediated  $Ca^{2+}$  Uptake and Limits Endothelial Cell Migration**

(A) Human peripheral veins were obtained from control and coronary/peripheral artery disease subjects (CAD/PAD). Freshly isolated ECs were cultured, and total RNA was used for detection of MICU1 and MCU mRNA expression levels by qRT-PCR. Mean  $\pm$  SEM; \* $p$  < 0.05; ns, not significant,  $n$  = 3–15.

(B and C) Confocal imaging and quantitation of basal  $[Ca^{2+}]_m$  accumulation as indicated by mitochondrial rhod-2 fluorescence in control, CVD, and CVD + MICU1 rescue ECs. Mean  $\pm$  SEM; \*\*\* $p$  < 0.001;  $n$  = 2–19 subjects.

(D) MICU1 protein expression in control and CVD ECs.

(E)  $I_{MCU}$  is larger in human-CVD-endothelial-cells-derived mitochondria. Traces are a representative single recording of  $I_{MCU}$ .  $n$  = 7–8.

(F) Average  $I_{MCU}$  densities at 5 mM  $Ca^{2+}$  in control and CVD ECs. Mean  $\pm$  SEM; \* $p$  < 0.05;  $n$  = 7–8.

(G and H) Representative images and quantitation of MitoSOX Red fluorescence (mROS indicator) in control, CVD, and CVD + MICU1 rescue ECs. Mean  $\pm$  SEM; \*\*\* $p$  < 0.001;  $n$  = 3–12.

(I and J) Representative images and quantitation of migratory scratch assay in CVD and CVD + MICU1 rescue ECs. Mean  $\pm$  SEM; \* $p$  < 0.05, \*\* $p$  < 0.01;  $n$  = 3–5.

higher current density (Figures 6E and 6F) suggesting that the increased  $Ca^{2+}$  uptake is a result of increased open probability of MCU due to lower expression of MICU1 (Figures 6A and 6D). Aberrant basal mitochondrial  $Ca^{2+}$  uptake may lead to mitochondrial oxidative stress in the form of superoxide, which is produced when electrons leak from the electron transport chain to react with molecular oxygen. Ablation of MICU1 in the EC cell line, EA.hy926, increased mitochondrial superoxide levels (Figures S4C–S4E). In CVD ECs, loss of MICU1 resulted in higher  $[Ca^{2+}]_m$ , through altered MCU-mediated mitochondrial  $Ca^{2+}$  uptake which subsequently increased basal superoxide levels (Figures 6G and 6H). We next tested whether elevated reactive oxygen species (ROS) from MICU1 knockdown lowers antioxi-

dant levels and alters EC proliferation (Balaban et al., 2005). Total reduced glutathione (GSH) content was assessed in EA.hy926 ECs expressing MICU1 shRNA or MICU1 shRNA + shRNA-insensitive MICU1. Reconstitution of MICU1 in MICU1 KD cells prevented the chronic ROS-induced reduction of GSH levels (Figures S4F and S4G). Further, reduced cell proliferation in MICU1-silenced ECs was restored by reconstitution with shRNA-insensitive MICU1cDNA (Figures S4H and S4I). Another key functional question is whether loss of MICU1 leads to altered angiogenesis in CVD. CVD-derived ECs exhibited diminished migration, which was rescued by stable expression of MICU1 (Figures 6I and 6J). We next tested whether CVD-derived ECs have an altered monocyte adhesion phenotype.

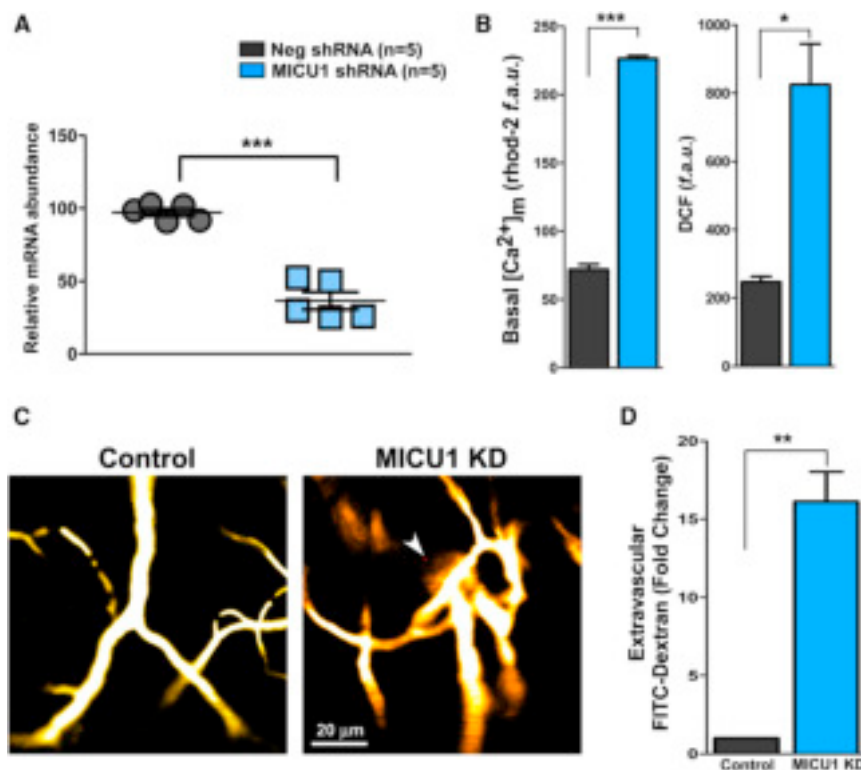


**Figure 7. In Vivo Knockdown of MICU1 Promotes Endothelial  $[Ca^{2+}]_m$  Accumulation, ROS Elevation, and Vascular Integrity Loss**

(A) Knockdown of MICU1 mRNA levels in mouse endothelial cells after MICU1 shRNA lentiviral delivery. Total mRNA was isolated from ECs, and qRT-PCR was performed. Mean  $\pm$  SEM; \*\*\*p < 0.001, n = 5.

(B) Quantitation of basal  $[Ca^{2+}]_m$  accumulation in control and MICU1KD mouse ECs (left panel). Quantitation of basal ROS levels in control and MICU1KD mouse ECs (right panel). Mean  $\pm$  SEM; \*p < 0.05, \*\*\*p < 0.001; n = 5.

(C) A 0.1–0.15 ml bolus of fluorescein isothiocyanate (FITC)-dextran (70 kDa, 5% w/v) was injected into the animals via facial vein. Anesthetized animals were placed under an intravital two-photon imaging system (Zeiss 710 META NLO), and images were acquired. Images are representative of multiple independent experiments. n = 5.

(D) Quantitation of vascular leakage was assessed as extravascular FITC-dextran fluorescence intensity. Mean  $\pm$  SEM; \*\*p < 0.01; n = 5.

We observed that CVD-derived ECs have an inherent propensity for monocyte adhesion (Figures S4J and S4K).

To explore the human MICU1 phenotype, we silenced MICU1 in mice and investigated the mitochondrial  $Ca^{2+}$  handling and vascular integrity. In vivo lentiviral delivery of MICU1 shRNA effectively knocked down MICU1 mRNA levels in ECs (Figure 7A). We also tested the MICU1 mRNA levels in cardiomyocytes, smooth muscle cells (SMCs), and splenocytes. Although SMCs and splenocytes, but not cardiomyocytes, showed partial knockdown of MICU1 following shRNA delivery, the MICU1 knockdown is more pronounced in ECs (Figure S5). Similar to cell-based and CVD-derived studies, downregulation of MICU1 expression promoted higher basal  $[Ca^{2+}]_m$  and ROS production (Figure 7B) culminating as a loss of vascular integrity (Figures 7C and 7D). Collectively, these results show that loss of MICU1 leads to aberrant EC mitochondrial  $Ca^{2+}$  handling and vascular pathology.

## DISCUSSION

These findings establish that mitochondrial matrix resident, MICU1, forms regulatory oligomers that require the MICU1 polybasic region for MCU binding and suppression of  $I_{MCU}$ . However, the polybasic region of MICU1 does not determine MICU1 oligomerization. Additionally, MICU1 EF hands which confer functional regulation of  $I_{MCU}$  do not determine MICU1/MCU complex formation. Our experiments also establish that the coiled-coil domains of MCU are essential for MICU1 binding.

Identifying the physiological function of protein regions remains a challenge for advanced bioinformatics and requires

conventional microscopy resolution limits. The major advantages of this method are that it is rapid, specific, real-time imaging, without RNAi silencing, subcellular fractionation, or antibodies, and it can resolve compartmentalization-determined protein functions such as residues of MCU accessible to MICU1. Taking the next step from localization, we show that the N-terminal region of the MICU1 polybasic motif determines MICU1/MCU binding. Whereas the polybasic motif has been previously reported to enhance protein-protein interaction (Williams, 2003), the polybasic motif is now identified in the mitochondria. The dominant negative MICU1- $\Delta$ K oligomer phenotype is likely a result of MICU1- $\Delta$ K interacting with wild-type MICU1, either sequestering wild-type MICU1 or causing a reduction of MICU1 oligomeric complex-binding affinity for MCU. Together, these data suggest that the polybasic region of MICU1 is not a MICU1/MCU interaction domain but supports the polybasic region's role in MCU interaction. The loss of MICU1 regulation by polybasic mutation could also be explained by diminished interaction of the polybasic mutant with the inner leaflet of the IMM. In support of this, the conserved polybasic region contains a glycine residue that could undergo myristoylation for membrane anchoring (Mumby et al., 1990; Thelen et al., 1991). This anchor could provide a mechanism for MICU1 to come on and off at active and resting state. This loose association is supported by our FRAP studies which show that MICU1 as a population is more mobile than MCU (Figure 1R). These critically important and diverse roles of the polybasic region and its role in mitochondrial  $Ca^{2+}$  signaling will certainly be elucidated in future studies.

Despite physiological mitochondrial  $Ca^{2+}$  uptake participates in mitochondrial bioenergetics and cellular  $Ca^{2+}$  signaling,

chronic  $\text{Ca}^{2+}$  accumulation is known to elicit mitochondrial dysfunction through mitochondrial permeability transition pore opening, mitochondrial ROS elevation, and cell death (Duchen et al., 2008; Hajnóczky et al., 2006). The mitochondrial  $\text{Ca}^{2+}$ -dependent cellular damage pathways are shared in many pathophysiological models, like cardiovascular disease, aging, and neurodegeneration (Davidson and Duchen, 2007). In cardiovascular diseases, the endothelium suffers from  $\text{Ca}^{2+}$ -dependent damage (Davidson and Duchen, 2007). Our results establish that endothelial cells derived from CVD subjects show low levels of MICU1 (Figures 6 and 7) and that the mitochondrial  $\text{Ca}^{2+}$ -uptake component of the disease phenotype can be reversed by the reconstitution of MICU1, thus restoring endothelial cell migration.

Collectively, we established a unique resolution-independent confocal technique to characterize the localization of complex components in viable organelles. Most importantly, we revealed that MICU1 interacts with MCU and regulates MCU-dependent  $[\text{Ca}^{2+}]_m$  uptake with a polybasic region and  $\text{Ca}^{2+}$ -sensing EF hand motifs. Additionally, we have shown that the coiled-coil domains of MCU interact with MICU1. Identification of these MICU1 and MCU domains provide the critical targets for mitochondrial  $\text{Ca}^{2+}$  uptake and potential therapeutic intervention in the pathogenesis of cardiovascular disease states.

## EXPERIMENTAL PROCEDURES

### Dynamic Protein Flux Assay

For all studies, MICU1, MCU, and other plasmid constructs were generated from human sequences. HeLa cells were cotransfected with cyto *c*-GFP and COX8A-mRFP (mitochondrial targeting sequence [MTS]), MICU1-YFP and COX8-mRFP, or MCU-GFP and COX8-mRFP plasmid constructs. Forty-eight hours posttransfection, cells were permeabilized with digitonin (0.002% w/v) for 7 min. Permeabilized cells were washed with digitonin-free intracellular-like medium supplemented with 2 mM succinate. After 100 s of baseline recording, permeabilized cells were exposed to either mastoparan (20  $\mu\text{g}/\text{ml}$ ) or alamethicin (20  $\mu\text{g}/\text{ml}$ ) at the indicated time points. Confocal images were recorded every 10 s (510 Meta; Carl Zeiss) at 488 and 561 nm excitation using a 40 $\times$  oil objective. Experiments were performed under pinhole settings of approximately 2.3  $\mu\text{m}$  to mitigate the impact of MICU1 rearrangement within the mitochondria. After completion of the time series, protein distribution maps were generated for before and after the mitochondrial membrane-permeabilizing agents. Images were analyzed, and flux rate was calculated. The colored histogram depiction represents the distribution of resolvable bit fluorescent intensities. Time is plotted from initial (top) to final (bottom) using the same individual experiment depicted in the representative individual trace. The intervals (bars) represent different time(s) during which the experiment was performed with the top bar indicating before the addition of either mastoparan or alamethicin. The protein flux images were analyzed using Zen 2010 software.

### FRAP Analysis

HeLa cells transfected with either MCU-GFP or MICU1-YFP were grown on glass coverslips for 48 hr before FRAP experiments. After baseline images were captured (one image/s), a small region (approximately 5% cytoplasmic area) was bleached with ten iterations of 488 nm at 100% laser power using a Zeiss 510 confocal microscope. Recordings of fluorescence recovery were captured for the following 45 s at 488 nm excitation. Recovery in the bleached region was the sum of all diffusing molecules, and normalized intensity was calculated as a percentage of the difference between the initial and bleached fluorescent arbitrary unit value.

### Measurement of Mitochondrial $\text{Ca}^{2+}$ Uptake and Mitochondrial Membrane Potential in Permeabilized Cell System

Control, MICU1- $\Delta\text{EF1}\Delta\text{EF2}$ , or MICU1- $\Delta\text{K}$  mutant HeLa cells were permeabilized using intracellular-like medium containing 2  $\mu\text{M}$  thapsigargin and 40  $\mu\text{g}/\text{ml}$  digitonin. The cell suspension supplemented with succinate (5 mM) was placed in a fluorimeter and permeabilized by gentle stirring. Fura-2FF (0.5  $\mu\text{M}$ ) was added at 0 s and JC-1 (800 nM) at 20 s to simultaneously measure extramitochondrial  $\text{Ca}^{2+}$  and  $\Delta\Psi_m$ , respectively. Fluorescence was monitored in a temperature-controlled (37 $^\circ\text{C}$ ) multiwavelength-excitation dual wavelength-emission spectrofluorometer (Delta RAM, Photon Technology International) using 490 nm excitation/535 nm emission for the monomer, 570 nm excitation/595 nm emission for the J-aggregate of JC-1, and 340 nm/380 nm for Fura-2FF. The ratiometric dye, Fura-2FF, was calibrated as previously described (Mallikankaraman et al., 2012b). At 450 s, 1  $\mu\text{M}$   $\text{Ca}^{2+}$  pulse was added and  $\Delta\Psi_m$  and extramitochondrial  $\text{Ca}^{2+}$  were monitored simultaneously. CCCP was added at 750 s to determine mitochondrial  $\text{Ca}^{2+}$  content.

### Mitoplast Patch-Clamp Recording

Mitoplast patch-clamp recordings were performed at 30 $^\circ\text{C}$  as detailed previously with modifications (Kirichok et al., 2004). Currents were recorded using a computer-controlled Axon200B patch-clamp amplifier with a Digidata 1320A acquisition board (pClamp 10.0 software; Axon Instruments). The ionic composition of the pipette (2, 5, and 100 mM  $\text{Ca}^{2+}$ ) was chosen based on previous measurements. Mitoplasts with p-orbital morphology were used for patch-clamp recording. Mitoplasts were bathed with a solution containing sodium gluconate (150 mM), KCl (5.4 mM),  $\text{CaCl}_2$  (5 mM), HEPES (10 mM), with a pH of 7.2. The pipette solution contained sodium gluconate (150 mM), NaCl (5 mM), sucrose (135 mM), HEPES (10 mM), and EGTA (1.5 mM), with a pH of 7.2. After formation of G $\Omega$  seals (pipette resistance 20–35 M $\Omega$ ), the mitoplasts were ruptured with 200–400 mV pulse varying from 2 to 6 ms duration. Mitoplast capacitance was measured (2.2–3.8 pF). After capacitance compensation, mitoplasts were held at 0 mV and  $I_{\text{MCU}}$  were elicited with a voltage ramp (from –160 mV to 80 mV, 120 mV/s).

### Isolation of Endothelial Cells from CVD and Control Subjects

Primary ECs were isolated from arteries and veins obtained from individuals undergoing surgical intervention for coronary artery disease (CAD)/peripheral artery disease (PAD) at the surgical unit of Temple University Hospital after due ethical clearance. The tissues were collected in standard EC transport medium and transported to the laboratory through cold chain and processed immediately. The tissues were initially washed once with PBS containing 100 U/ml penicillin and 100  $\mu\text{g}/\text{ml}$  streptomycin and then cleaned to remove the fibrous portion with sterile forceps. Using a sterile blade, the veins were cut vertically and carefully flipped over. The tissues were cut into small squares of approximately 0.5 cm  $\times$  0.5 cm and placed in a 100 mm dish with medium just bathing the tissue pieces. The plates were incubated at 37 $^\circ\text{C}$ , 5%  $\text{CO}_2$ . After 1 week, the tissue pieces were removed leaving the individual colonies to develop into a confluent monolayer. Endothelial cell phenotypes were characterized as previously described (Milovanova et al., 2008).

### Endothelial Migration Assay

Control, CVD-derived ECs, and CVD + MICU1 rescue ECs were seeded at a density of  $1 \times 10^5$  cells/well in 6-well plates overnight for confluent monolayer. A uniform 1.8 mm scratch running the entire length of the well was created using a sterile 200  $\mu\text{l}$  tip. The wells were washed three times with PBS to remove the cell debris and then bathed in 2 ml complete endothelial medium. After 24 hr, cells were washed and fixed with CAMCO Quick Stain II as per manufacturer instructions. The wells were photographed at multiple locations using phase contrast microscopy with a 4 $\times$  objective. Migration was quantified using Image J software (National Institutes of Health); results are expressed as percent gap closure (Craige et al., 2011).

### In Vivo Knockdown of MICU1 and Vascular Integrity Measurement

To knock down MICU1 in control mice, we used lentivirus carrying MICU1-shRNA. Three daily doses of MICU1-shNRA ( $1 \times 10^8$  TU/ml as measured by p24 ELISA and also confirmed by true infectious titer via puromycin resistance in EC culture; 100  $\mu\text{l}/\text{mice}$  was delivered using saline as vehicle) lentivirus or

control lentivirus-negative shRNA were administered intravenously, and MICU1 expression in the endothelial cells, cardiomyocytes, SMCs, and splenocytes were assessed by qRT-PCR after 5 days from the last injection (8 total days). Freshly isolated primary ECs were rapidly subjected to  $[Ca^{2+}]_m$  and ROS measurement. The vascular integrity studies were performed as described previously (Gandhirajan et al., 2013).

### Statistical Analysis

Data were expressed as the means  $\pm$  SE. Statistical significance was evaluated via one-way ANOVA and Student's *t* test. A *p* value of  $<0.05$  was considered statistically significant. All experiments were conducted at least three times unless specified. Data were plotted either with GraphPad Prism version 5.0 or with Sigma Plot 11.0 software.

### SUPPLEMENTAL INFORMATION

Supplemental Information includes Supplemental Experimental Procedures, five figures, and one table and can be found with this article online at <http://dx.doi.org/10.1016/j.celrep.2013.11.026>.

### ACKNOWLEDGMENTS

We thank Douglas R. Green for cytochrome *c*-GFP plasmid construct. We thank Kevin J. Foskett, Donald L. Gill, and Walter J. Koch for comments on the manuscript. This research was funded by the National Institutes of Health (HL086699, HL109920, and 1S10RR027327-01).

Received: August 22, 2013

Revised: October 28, 2013

Accepted: November 14, 2013

Published: December 12, 2013

### REFERENCES

Aichberger, K.J., Mittermann, I., Reininger, R., Seiberler, S., Swoboda, I., Spitzauer, S., Kopp, T., Stingl, G., Sperr, W.R., Valent, P., et al. (2005). Hom s 4, an IgE-reactive autoantigen belonging to a new subfamily of calcium-binding proteins, can induce Th cell type 1-mediated autoreactivity. *J. Immunol.* *175*, 1286–1294.

Babcock, D.F., Herrington, J., Goodwin, P.C., Park, Y.B., and Hille, B. (1997). Mitochondrial participation in the intracellular  $Ca^{2+}$  network. *J. Cell Biol.* *136*, 833–844.

Baines, C.P., Kaiser, R.A., Purcell, N.H., Blair, N.S., Osinska, H., Hambleton, M.A., Brunskill, E.W., Sayen, M.R., Gottlieb, R.A., Dorn, G.W., et al. (2005). Loss of cyclophilin D reveals a critical role for mitochondrial permeability transition in cell death. *Nature* *434*, 658–662.

Balaban, R.S. (2009). The role of  $Ca^{2+}$  signaling in the coordination of mitochondrial ATP production with cardiac work. *Biochim. Biophys. Acta* *1787*, 1334–1341.

Balaban, R.S., Nemoto, S., and Finkel, T. (2005). Mitochondria, oxidants, and aging. *Cell* *120*, 483–495.

Baughman, J.M., Perocchi, F., Girgis, H.S., Plovanich, M., Belcher-Timme, C.A., Sancak, Y., Bao, X.R., Strittmatter, L., Goldberger, O., Bogorad, R.L., et al. (2011). Integrative genomics identifies MCU as an essential component of the mitochondrial calcium uniporter. *Nature* *476*, 341–345.

Bernardi, P. (1999). Mitochondrial transport of cations: channels, exchangers, and permeability transition. *Physiol. Rev.* *79*, 1127–1155.

Berridge, M.J., Bootman, M.D., and Roderick, H.L. (2003). Calcium signalling: dynamics, homeostasis and remodelling. *Nat. Rev. Mol. Cell Biol.* *4*, 517–529.

Cárdenas, C., Miller, R.A., Smith, I., Bui, T., Molgó, J., Müller, M., Vais, H., Cheung, K.H., Yang, J., Parker, I., et al. (2010). Essential regulation of cell bioenergetics by constitutive InsP3 receptor  $Ca^{2+}$  transfer to mitochondria. *Cell* *142*, 270–283.

Chaudhuri, D., Sancak, Y., Mootha, V.K., and Clapham, D.E. (2013). MCU encodes the pore conducting mitochondrial calcium currents. *eLife* *2*, e00704.

Clapham, D.E. (2007). Calcium signaling. *Cell* *131*, 1047–1058.

Craige, S.M., Chen, K., Pei, Y., Li, C., Huang, X., Chen, C., Shibata, R., Sato, K., Walsh, K., and Keaney, J.F., Jr. (2011). NADPH oxidase 4 promotes endothelial angiogenesis through endothelial nitric oxide synthase activation. *Circulation* *124*, 731–740.

Csordás, G., Golenár, T., Seifert, E.L., Kamer, K.J., Sancak, Y., Perocchi, F., Moffat, C., Weaver, D., de la Fuente Perez, S., Bogorad, R., et al. (2013). MICU1 controls both the threshold and cooperative activation of the mitochondrial  $Ca^{2+}$  uniporter. *Cell Metab.* *17*, 976–987.

Davidson, S.M., and Duchen, M.R. (2007). Endothelial mitochondria: contributing to vascular function and disease. *Circ. Res.* *100*, 1128–1141.

De Stefani, D., Raffaello, A., Teardo, E., Szabò, I., and Rizzuto, R. (2011). A forty-kilodalton protein of the inner membrane is the mitochondrial calcium uniporter. *Nature* *476*, 336–340.

Denton, R.M., and McCormack, J.G. (1980). The role of calcium in the regulation of mitochondrial metabolism. *Biochem. Soc. Trans.* *8*, 266–268.

Drago, I., Pizzo, P., and Pozzan, T. (2011). After half a century mitochondrial calcium in- and efflux machineries reveal themselves. *EMBO J.* *30*, 4119–4125.

Duchen, M.R., Verkhratsky, A., and Muallem, S. (2008). Mitochondria and calcium in health and disease. *Cell Calcium* *44*, 1–5.

Fieni, F., Lee, S.B., Jan, Y.N., and Kirichok, Y. (2012). Activity of the mitochondrial calcium uniporter varies greatly between tissues. *Nature communications* *3*, 1317.

Gandhirajan, R.K., Meng, S., Chandramoorthy, H.C., Mallikankaraman, K., Mancarella, S., Gao, H., Razmpour, R., Yang, X.F., Houser, S.R., Chen, J., et al. (2013). Blockade of NOX2 and STIM1 signaling limits lipopolysaccharide-induced vascular inflammation. *J. Clin. Invest.* *123*, 887–902.

Gunter, T.E., Gunter, K.K., Sheu, S.S., and Gavin, C.E. (1994). Mitochondrial calcium transport: physiological and pathological relevance. *Am. J. Physiol.* *267*, C313–C339.

Hajnóczky, G., Robb-Gaspers, L.D., Seitz, M.B., and Thomas, A.P. (1995). Decoding of cytosolic calcium oscillations in the mitochondria. *Cell* *82*, 415–424.

Hajnóczky, G., Csordás, G., Das, S., Garcia-Perez, C., Saotome, M., Sinha Roy, S., and Yi, M. (2006). Mitochondrial calcium signalling and cell death: approaches for assessing the role of mitochondrial  $Ca^{2+}$  uptake in apoptosis. *Cell Calcium* *40*, 553–560.

Hancock, J.F., Paterson, H., and Marshall, C.J. (1990). A polybasic domain or palmitoylation is required in addition to the CAAX motif to localize p21ras to the plasma membrane. *Cell* *63*, 133–139.

Hansford, R.G. (1994). Physiological role of mitochondrial  $Ca^{2+}$  transport. *J. Bioenerg. Biomembr.* *26*, 495–508.

Heo, W.D., Inoue, T., Park, W.S., Kim, M.L., Park, B.O., Wandless, T.J., and Meyer, T. (2006). PI(3,4,5)P3 and PI(4,5)P2 lipids target proteins with polybasic clusters to the plasma membrane. *Science* *314*, 1458–1461.

Joiner, M.L., Koval, O.M., Li, J., He, B.J., Allamargot, C., Gao, Z., Luczak, E.D., Hall, D.D., Fink, B.D., Chen, B., et al. (2012). CaMKII determines mitochondrial stress responses in heart. *Nature* *491*, 269–273.

Kirichok, Y., Krapivinsky, G., and Clapham, D.E. (2004). The mitochondrial calcium uniporter is a highly selective ion channel. *Nature* *427*, 360–364.

Kluck, R.M., Esposito, M.D., Perkins, G., Renken, C., Kuwana, T., Bossy-Wetzel, E., Goldberg, M., Allen, T., Barber, M.J., Green, D.R., and Newmeyer, D.D. (1999). The pro-apoptotic proteins, Bid and Bax, cause a limited permeabilization of the mitochondrial outer membrane that is enhanced by cytosol. *J. Cell Biol.* *147*, 809–822.

Lemasters, J.J., Theruvath, T.P., Zhong, Z., and Nieminen, A.L. (2009). Mitochondrial calcium and the permeability transition in cell death. *Biochim. Biophys. Acta* *1787*, 1395–1401.

Libby, P., Aikawa, M., and Jain, M.K. (2006). Vascular endothelium and atherosclerosis. *Handbook Exp. Pharmacol.* *2006*, 285–306.

- Mallilankaraman, K., Cárdenas, C., Doonan, P.J., Chandramoorthy, H.C., Irrinki, K.M., Golenár, T., Csordás, G., Madireddi, P., Yang, J., Müller, M., et al. (2012a). MCUR1 is an essential component of mitochondrial Ca<sup>2+</sup> uptake that regulates cellular metabolism. *Nat. Cell Biol.* **14**, 1336–1343.
- Mallilankaraman, K., Doonan, P., Cárdenas, C., Chandramoorthy, H.C., Müller, M., Miller, R., Hoffman, N.E., Gandhirajan, R.K., Molgó, J., Birnbaum, M.J., et al. (2012b). MICU1 is an essential gatekeeper for MCU-mediated mitochondrial Ca<sup>2+</sup> uptake that regulates cell survival. *Cell* **151**, 630–644.
- McCormack, J.G., Halestrap, A.P., and Denton, R.M. (1990). Role of calcium ions in regulation of mammalian intramitochondrial metabolism. *Physiol. Rev.* **70**, 391–425.
- Milovanova, T., Chatterjee, S., Hawkins, B.J., Hong, N., Sorokina, E.M., Debolt, K., Moore, J.S., Madesh, M., and Fisher, A.B. (2008). Caveolae are an essential component of the pathway for endothelial cell signaling associated with abrupt reduction of shear stress. *Biochim. Biophys. Acta* **1783**, 1866–1875.
- Mumby, S.M., Heukeroth, R.O., Gordon, J.I., and Gilman, A.G. (1990). G-protein alpha-subunit expression, myristoylation, and membrane association in COS cells. *Proc. Natl. Acad. Sci. USA* **87**, 728–732.
- Nicholls, D.G. (1978). The regulation of extramitochondrial free calcium ion concentration by rat liver mitochondria. *Biochem. J.* **176**, 463–474.
- Nicholls, D.G. (2005). Mitochondria and calcium signaling. *Cell Calcium* **38**, 311–317.
- Orrenius, S., Zhivotovsky, B., and Nicotera, P. (2003). Regulation of cell death: the calcium-apoptosis link. *Nat. Rev. Mol. Cell Biol.* **4**, 552–565.
- Papayannopoulos, V., Co, C., Prehoda, K.E., Snapper, S., Taunton, J., and Lim, W.A. (2005). A polybasic motif allows N-WASP to act as a sensor of PIP(2) density. *Mol. Cell* **17**, 181–191.
- Perocchi, F., Gohil, V.M., Girgis, H.S., Bao, X.R., McCombs, J.E., Palmer, A.E., and Mootha, V.K. (2010). MICU1 encodes a mitochondrial EF hand protein required for Ca<sup>2+</sup> uptake. *Nature* **467**, 291–296.
- Pfeiffer, D.R., Gudiz, T.I., Novgorodov, S.A., and Erdahl, W.L. (1995). The peptide mastoparan is a potent facilitator of the mitochondrial permeability transition. *J. Biol. Chem.* **270**, 4923–4932.
- Rizzuto, R., De Stefani, D., Raffaello, A., and Mammucari, C. (2012). Mitochondria as sensors and regulators of calcium signalling. *Nat. Rev. Mol. Cell Biol.* **13**, 566–578.
- Santo-Domingo, J., and Demaurex, N. (2010). Calcium uptake mechanisms of mitochondria. *Biochim. Biophys. Acta* **1797**, 907–912.
- Soboloff, J., Rothberg, B.S., Madesh, M., and Gill, D.L. (2012). STIM proteins: dynamic calcium signal transducers. *Nat. Rev. Mol. Cell Biol.* **13**, 549–565.
- Szalai, G., Krishnamurthy, R., and Hajnóczky, G. (1999). Apoptosis driven by IP(3)-linked mitochondrial calcium signals. *EMBO J.* **18**, 6349–6361.
- Thelen, M., Rosen, A., Nairn, A.C., and Aderem, A. (1991). Regulation by phosphorylation of reversible association of a myristoylated protein kinase C substrate with the plasma membrane. *Nature* **351**, 320–322.
- Williams, C.L. (2003). The polybasic region of Ras and Rho family small GTPases: a regulator of protein interactions and membrane association and a site of nuclear localization signal sequences. *Cell. Signal.* **15**, 1071–1080.
- Williams, G.S., Boyman, L., Chikando, A.C., Khairallah, R.J., and Lederer, W.J. (2013). Mitochondrial calcium uptake. *Proc. Natl. Acad. Sci. USA* **110**, 10479–10486.